Fermi National Accelerator Laboratory

FERMILAB-Pub-79/59-EXP
7420.546
(Submitted to Phys. Rev.)

DIMUON PRODUCTION BY NEUTRINOS IN THE FERMILAB 15-FOOT BUBBLE CHAMBER

H. C. Ballagh, H. H. Bingham, W. B. Fretter, T. Lawry
G. R. Lynch, J. Lys, J. P. Marriner, J. Orthel,
M. D. Sokoloff, M. L. Stevenson, G. P. Yost
Department of Physics and Lawrence Berkeley Laboratory
University of California, Berkeley, California 94720

and

B. Chrisman, D. Gee, A. Greene, G. Harigel, F. F. Huson
T. Murphy, E. Schmidt, W. Smart, E. Treadwell, J. Wolfson
Fermi National Accelerator Laboratory, Batavia, Illinois 60510

and

R. J. Cence, F. A. Harris, M. D. Jones
S. I. Parker, M. W. Peters, V. Z. Peterson
University of Hawaii at Manoa, Honolulu, Hawaii 96822

and

T. H. Burnett, L. Fluri, D. Holmgren, H. J. Lubatti,
K. Moriyasu, D. Rees, H. Rudnicka, G. M. Swider, E. Wolin
University of Washington, Seattle, Washington 98195

and

R. Benada, U. Camerini, M. Duffy, W. Fry
R. J. Loveless, P. McCable, D. D. Reeder
University of Wisconsin, Madison, Wisconsin 53706

July 1979

DIMUON PRODUCTION BY NEUTRINOS IN THE FERMILAB 15-FOOT BUBBLE CHAMBER

H. C. Ballagh, H. H. Bingham, W. B. Fretter, T. Lawry,
G. R. Lynch, J. Lys, J. P. Marriner,[a] J. Orthel,
M. D. Sokoloff, M. L. Stevenson, G. P. Yost

Department of Physics and Lawrence Berkeley Lab
University of California, Berkeley
Berkeley, California 94720

B. Chrisman, D. Gee, A. Greene,[b] G. Harigel,[c] F. R. Huson,
T. Murphy, E. Schmidt, W. Smart, E. Treadwell, J. Wolfson

FERMILAB
P. O. Box 500
Batavia, Illinois 60510

R. J. Cence, F. A. Harris, M. D. Jones,
S. I. Parker, M. W. Peters, V. Z. Peterson

Department of Physics
University of Hawaii at Manoa
Honolulu, Hawaii 96822

T. H. Burnett, L. Fluri, D. Holmgren, H. J. Lubatti,
K. Moriyasu, D. Rees, H. Rudnicka, G. M. Swider, E. Wolin

Visual Techniques Lab, Department of Physics
University of Washington
Seattle, Washington 98195

R. Benada, U. Camerini, M. Duffy, W. Fry,
R. J. Loveless, P. McCabe, D. D. Reeder

Department of Physics
University of Wisconsin
Madison, Wisconsin 53706

---

[a] Present address: FERMILAB, P. O. Box 500, Batavia, Illinois 60510.

[b] Present address: Brookhaven National Laboratory, Upton, L.I., New York 11973.

[c] Present address: CERN, 1211 Geneva 23, Switzerland.

Abstract

In a 326,000 picture exposure of the Fermilab 15' Neon-Hydrogen Bubble Chamber to the Quadrupole Triplet Neutrino Beam, 62 dimuon candidates have been found: 0 $\mu^+\mu^+$, 54 $\mu^-\mu^+$ and $\mu^+\mu^-$, and 8 $\mu^-\mu^-$. The $\mu^-\mu^-$ candidates are consistent with background. The ratio of opposite-sign dimuon events to single muon events is $(0.39 \pm 0.10) \times 10^{-2}$ for a muon momentum cut of 4 GeV/c. There are 10 V^0 in the opposite-sign dimuon events, yielding a neutral strange particle rate per event of 0.6 ± 0.3.

I. *Introduction*

The dominant mechanism for the production of dimuon events in neutrino interactions[1-9] is believed to be charmed particle production followed by semi-leptonic decay. We have employed the Fermilab 15' Bubble Chamber exposed to a high-energy-enhanced neutrino beam to examine the evidence for this mechanism and explore for new phenomena. Half (one-quarter) of the charged-current neutrino interactions have energies above 70 GeV (115 GeV). Until recently, bubble chamber experiments, which can examine the details of the final hadronic state (for instance, the number of neutral strange particles (V^0) produced), have primarily studied the corresponding decay into an electron.[10-14] Now with improved muon identification, it is also possible for bubble chamber experiments to study dimuon events,[7-9] allowing the simultaneous comparison of the two samples in the same detector and with the same beam. In this paper, we present results on dimuon events; the electron results will be published later. Just as with earlier experiments,[1-14] we have found evidence for charm production. Details are given in Section VI. The description of the apparatus, the technique of finding and selecting events, calculation of background, and the determination of the detection efficiency and rates are given in Sections II-V, respectively.

II. Apparatus

The experiment was carried out using the Fermilab 15' Bubble Chamber, plus a two-plane External Muon Identifier (EMI). The bubble chamber liquid was a neon (47% atomic)-hydrogen mix, which had a density, radiation length, and absorption length of 0.56 g/cm^3, 53 cm, and 193 cm respectively. The

two-plane EMI,[15] which was of prime importance to the dimuon search, was an expansion and reconfiguration of the original one-plane EMI,[16] and had 18 one-meter-square multiwire proportional chambers in the first plane and 21 in the second plane. Additional concrete and lead were placed between the two planes, so that muons traverse a total of 7 to 11 absorption lengths before reaching the second plane. The bubble chamber and EMI arrangement are shown in Fig. 1.

The bubble chamber was exposed to the Quadrupole Triplet Neutrino Beam. In this beam, charged pions and kaons produced at the target are focused with conventional quadrupole magnets. The target used was one interaction length of alumina, and the 400 GeV/c incident proton beam had a typical intensity of 10^{13} protons per pulse. The ratio of ν- to $\bar{\nu}$-induced events in this beam is approximately 6 to 1. This beam emphasizes high energy neutrinos (the average neutrino event energy is 90 GeV) and has a long spill (2 millisecs) which is important in eliminating accidental time-coincident EMI background in the dimuon sample. The energy spectra for neutrinos and antineutrinos in this beam are shown in Fig. 2.[17] A total of 326,000 good neutrino pictures with EMI information was obtained, corresponding to 3.4×10^{18} protons on target.

III. Scanning, Event Selection, and Cuts

The film was scanned for all neutral-induced events. In a rescan of 20% of the film, the scanning efficiency for EMI identified charged-current events was found to be 98%. The first measurement pass consisted of measuring all non-interacting tracks leaving the bubble chamber with an angle from the neutrino direction of less than 60°. These tracks were then

extrapolated to the EMI planes and the predicted EMI positions were compared with the positions of fitted coordinates (fits) in the EMI chambers in order to identify muons and hence to select neutrino and antineutrino charged-current events and candidate dimuon events. Events were required to be in a restricted fiducial volume (17.6 m^3), having a minimum potential length to the downstream wall of 50 cm. Muons in charged-current events were required to have time-coincident matches (within 400 nsec) in each plane with a combined two-plane confidence level, describing the goodness of fit of the EMI matches, greater than 10^{-4}. Muons in candidate dimuon events were required to have combined two-plane confidence levels greater than 1%. Correlations between the hit positions in the two planes were taken into account in calculating these confidence levels. Because of $\pi \to \mu\nu$ and $K \to \mu\nu$ background in dimuon events, only muons with momentum greater than 4 GeV/c were considered in this paper.

A total of 10,260 neutrino and 1,770 antineutrino charged-current (CC) events and 62 dimuon candidates were identified (all with muon momentum greater than 4 GeV/c). All dimuon candidates were fully measured, as well as an unbiased sample of 600 neutrino CC events and 300 antineutrino CC events for comparison. The measurements included neutral interactions, V^0's, and converted gammas within 2 radiation lengths of the primary vertex.

IV. Backgrounds

In this section possible backgrounds to the dimuon candidates from ordinary CC events are considered. Backgrounds from neutral-current events and from neutral-hadron-induced events are negligible. The hadron contamination of the single muon sample with the loose confidence level cut used is approximately 1%, which is negligible for the purposes of this paper.

A) Accidentals

Because of the long spill, 2-3 millisec, and small coincidence window (400 ns), the time-coincident accidental background was expected to be very small. An experimental check of this has been made by analyzing a subsample of events using EMI information from another frame. No fake dimuon events were found using a 10^{-4} two-plane confidence level cut, implying less than 1 event background from this source in the entire sample with a 1% two-plane confidence level cut.

B) Decays

The most serious background in the dimuon sample arises from normal charged-current events in which a produced π or K decays into a muon and neutrino. These decays also provide the most serious background in counter experiments. However, two differences should be noted. In the bubble chamber, only pions and kaons produced in the initial neutrino interaction need be considered, and not those from secondary hadron interactions. On the other hand, the bubble chamber provides a relatively long flight path in low density material and hence there is a greater probability of a meson decaying before interaction. Most decays in the bubble chamber are not visually recognizable because of the small changes in angle and curvature. The track that is measured and then extrapolated is therefore a composite of parent meson and daughter muon.

The basic information for calculating the decay background comes from the leaving track measurements: the number of leaving prongs and the momentum and spatial distribution of these prongs. From this information and the estimated number of π and K leaving tracks in the leaving track sample, the number of decays is calculated using the known lifetimes and the interaction lengths of the bubble-chamber

liquid and EMI absorber. However, not all of these decays will be accepted into our final sample. Factors which reduce this background are: a) some decay muons will miss the EMI, b) some tracks will be lost due to EMI instrumental inefficiency, c) some tracks decaying inside the bubble chamber will yield a fitted momentum less than 4 GeV/c, d) some tracks will fail reconstruction in geometry or give a visible kink in the bubble chamber, e) many will yield a low two-plane confidence level.

A Monte Carlo program has been used to generate points in space along the π (or K) and μ track segments for decays inside the bubble chamber in order to estimate some of these factors. The measurements are processed with a geometry program,[18] which fits a single curve to the composite track made up of the two segments. The fitted track and the decay muon track are extrapolated to the EMI to determine the EMI confidence level. The effect of multiple Coulomb scattering of the muon track is included. For $\pi \to \mu\nu$ ($K \to \mu\nu$), 40% (65%) of the decays have an EMI confidence level less than 1%, and including all factors, 44% (75%) of the decays are eliminated.

To reduce the background further, identification of decays inside the bubble chamber has been attempted. A procedure for cutting back tracks, which is designed to detect significant energy loss, has been used. The momentum over the first half of a track is compared with that for the last half of a track. If the initial momentum is greater by more than one standard deviation, the track is cut back, 10% at a time, until the two momenta are within one standard deviation. The same Monte Carlo generated decays were used to calibrate the sensitivity of this procedure for identifying decays. If only cut-back tracks with a 1 micron improvement in residuals are considered to be

identified, then 18% of those π-μ decays surviving all other cuts are eliminated, while only 2% of non-decay tracks are eliminated. A total of 5 events are eliminated by this cut compared to the predicted loss of 3.1 events: 1.3 real dimuon events and 1.8 decay background events.

The final background estimate, which is shown in Table I, is made assuming that the leaving tracks contain 6% kaons and that the positive leaving tracks contain 5% protons; the remainder being pions.[19] The error of 20% on this estimate comes from two sources: an uncertainty in the kaon to pion ratio contributes a 10% error and differences in the geometrical reconstructions at the five laboratories contribute the remainder.

C) Punch Thru

Leaving hadrons may fake muons because either they penetrate the EMI absorber directly or their tracks give accidental spatial coincidences with in-time fits in one or both EMI planes. For simplicity, we group these two components together under the name "punch thru." There are many sources of time-coincident EMI fits. Such fits are produced by decays of pion and kaon secondaries inside the EMI absorber as well as by remnants of hadronic showers from this track and all other tracks in the event, by delta-rays accompanying the primary muon, and by creation of spurious solutions from raw EMI encodings. Penetrating hadrons will have closely associated fits in the EMI, while the accidental spatial coincidences will be more diffuse. This diffuseness is expected even for the shower of the hadron itself because the angles of hadronic interactions are large compared to the multiple Coulomb scattering angles.

The background due to penetrating hadrons is estimated by extrapolating (exponentially) the amount of closely associated component observed in the

first EMI plane into the second EMI plane. The estimated background is less than one event, as expected, since the EMI absorber is 7 to 11 collision lengths thick.

The background from accidental matches is determined using all tracks other than primary muon tracks with a good match in the first EMI plane. In the second EMI plane, the in-time background in a small region about these extrapolated tracks (within 60 cm) is nearly uniform outside the region of the signal peak. We then calculate the background assuming the in-time background extrapolates uniformly under the signal peak. The total estimated background from this source is given in Table I,[20] along with a 50% uncertainty which results from the uncertainty in the extrapolation and from the statistical error.

V. Efficiencies and Rates

The number of candidate events found and the estimated backgrounds are presented in Table I. A total of 36 opposite-sign dimuons remain after background subtraction. In order to determine the rates, the geometric acceptances for samples of neutrino and antineutrino charged-current events and dimuons have been calculated by moving the events randomly about the bubble chamber, weighting them to give agreement with the observed spatial distribution of events, and rotating them randomly about the neutrino direction. The average acceptances for the samples were found to be 85 ± 4% (ν), 91 ± 4% ($\bar{\nu}$), and 74 ± 5% (dimuons). For the mixture of neutrino-induced and antineutrino-induced dimuon events, we define

$$R = \frac{\text{Rate } (\nu + N \to \mu^- \mu^+ X) + \text{Rate } (\bar{\nu} + N \to \mu^+ \mu^- X)}{\text{Rate } (\nu + N \to \mu^- X) + \text{Rate } (\bar{\nu} + N \to \mu^+ X)} .$$

Correcting for loss of dimuons due to leaving tracks missed in scanning (3%), the confidence level cut (6%), the cutting-back procedure to identify decays (4%), and the geometric acceptance and instrumental inefficiency, we find

$$R = (0.39 \pm 0.10) \times 10^{-2} .$$

This rate is for muons with momentum greater than 4 GeV/c.

In order to separate neutrino-induced and antineutrino-induced dimuon events, we define the muon with the largest transverse momentum relative to all other non-muon tracks to be the primary muon (coming from the neutrino vertex). Our charm production and decay Monte Carlo (described below) predicts that this method of selection is correct 95% (91%) of the time for ν ($\bar{\nu}$) events. In Fig. 3, a plot of the transverse momentum of the primary muon versus that of the secondary muon is shown. Most events are well separated from the diagonal, where the choice is ambiguous. Allowing for misidentification of the primary muon and subtracting backgrounds, we estimate that there are 30.3 $\mu^-\mu^+$ events (neutrino-induced) and 5.7 $\mu^+\mu^-$ events (antineutrino-induced) in the sample. Correcting for lost events and the detection efficiency (acceptance × instrumental efficiency) of muons above 4 GeV/c, we find

$$R^{-+} = \frac{\text{Rate } (\nu + N \to \mu^-\mu^+X)}{\text{Rate } (\nu + N \to \mu^-X)}$$

$$= (0.37 \pm 0.10) \times 10^{-2}$$

$$R^{+-} = \frac{\text{Rate } (\bar{\nu} + N \to \mu^+\mu^-X)}{\text{Rate } (\bar{\nu} + N \to \mu^+X)}$$

$$= (0.5 \pm 0.3) \times 10^{-2}$$

According to our charm production and decay Monte Carlo, approximately 40% of dimuons have been lost because of the 4 GeV/c muon momentum requirement. Taking this loss into account, our R^{-+} agrees with the corresponding μ^-e^+ rate measured in another experiment,[12] 0.5 ± 0.15, even though the energy spectra of the two beams are quite different.

A more direct comparison can be made with the dimuon experiment of Ref. 4, which presents R^{-+} as a function of neutrino energy. Their dimuon acceptance is determined primarily by their 4.5 GeV/c muon momentum requirement, which is very similar to our momentum requirement. Using their data, we have calculated what R^{-+} we would expect for our energy spectrum and find a value of 0.35 ± 0.04. This is in excellent agreement with our measurement, even though the systematic uncertainties of the two experiments are quite different. Dividing our events into two energy regions, we find $R(E_\nu < 100$ GeV) = $(0.30 \pm 0.10) \times 10^{-2}$ and $R(E_\nu > 100$ GeV) = (0.55 ± 0.18). These are also in excellent agreement with Ref. 4. The difference in R in these two energy regions may be attributed primarily to the 4 GeV/c muon momentum requirement.

The same-sign dimuon candidates are consistent with being all background. The 90% confidence level upper limit for the number of actual $\mu^-\mu^-$ events is 6.8. The 90% confidence limit for the ratio of $\mu^-\mu^-$ events to $\mu^-\mu^+$ events (R^{--}/R^{-+}) is 0.27. This is not in disagreement with the ratio of 0.06 ± 0.05 (0.12 ± 0.05 for muon momentum above 10 GeV/c) quoted in Ref. 5.

Of special interest is the strange particle rate in the dimuon events since in the charm model an enhanced rate is expected. There are 10 V^o events yielding good 3-constraint kinematic fits in the sample of opposite-sign dimuon events. Their characteristics are presented in Table II. All of the V^o's

unambiguously fit K^o or Λ^o, giving a total of 8 K^o's and 2 Λ^o's for a raw V^o rate of 19 ± 5% in the dimuon sample (including background). In order to correct for detection efficiency, we weight each event by the reciprocal of its detection probability including EMI acceptance and such effects as interaction before decay and decays too close to the primary vertex (1 cm), outside the chamber, or too close to the wall of the bubble chamber (20 cm). V^o's are required to be 1 cm from the primary vertex because of the uncertain detection efficiency for V^o's closer than this. We assume 100% efficiency beyond this distance for dimuon events. Two V^o's decay within 1 cm of the primary vertex, so no weight is calculated for them. Another two V^o's have relatively high weights because their high momenta (39 and 55 GeV/c) give large probabilities of leaving the bubble chamber before decay.

A sample of neutrino charged-current events has been used to determine the V^o content of the background events. For each event, we have calculated a background probability which is the sum of the decay probability and punch thru probability summed over all leaving tracks in the event. The V^o fraction for background events is given by the sum of the background probabilities of the V^o events divided by the sum of the background probabilities of all events. The raw V^o fraction in the background events is found to be 11 ± 2% per event, which is not very different from the V^o fraction in the neutrino charged-current sample, 10.5 ± 1.5%. The dimuon sample has a higher V^o rate, even before correcting for background. Subtracting background, weighting for detection, and correcting for unseen decays, we find a ratio ($\mu\mu V^o X/\mu\mu X$) of 0.6 ± 0.3. This is in good agreement with the corrected V^o ratio of 0.6 ± 0.2 in μe events of Ref. 12.

VI. Experimental Distributions and Comparison with Charm Model

The dimuon events and an unbiased sample of charged-current events have been measured fully, including neutral interactions, decays, and all converted gammas within two radiation lengths of the primary vertex. The neutrino energy, E_ν, is estimated by summing the momenta along the neutrino direction. An average correction to account for missing neutrals is applied to the sum of the longitudinal momentum of all tracks other than the primary muon, P_x^o. The correction[21] was determined from the imbalance of the mean transverse momentum of the primary muon and the mean transverse momentum of all other tracks as a function of P_x^o and is well parametrized by

$$P_x^o\Big|_{\text{corrected}} = A\, P_x^o + B,$$

where $A = 1.16 \pm 0.03$ and $B = 3.3 \pm 0.5$ GeV/c for the sample of neutrino charged-current events and $A = 1.28 \pm 0.06$ and $B = 2.1 \pm 1.6$ GeV/c for the dimuon events. The multiplicative correction is higher for dimuons, indicating a greater missing energy, but the uncertainties are large.

The correction obtained for the charged-current events agrees well with the result of a test of the energy resolution of the bubble chamber using 25 GeV π^-'s on a somewhat denser neon-hydrogen mixture. The bubble chamber measured on the average 87 ± 2% of the incident pion energy.

For the distributions, we have identified neutrino-induced and antineutrino-induced dimuon events using a method similar to the separation method discussed earlier. In order to reduce the background due to misidentified $\mu^-\mu^+$ events, we require for an event to be called a $\mu^+\mu^-$ event that the transverse momentum of the μ^+ must be 1.4 GeV/c greater than that of the μ^-. The samples selected in this manner have approximately the same purity.

The contribution to each distribution from background events in the dimuon sample has been calculated from the CC sample, weighting each event by the punch thru and decay probabilities summed over all tracks.

In order to compare our experimental data with what is expected on the basis of a charm model, we have written a Monte Carlo program based on that of Ref. 22. The program simulates the production of a charmed quark either by a neutrino or antineutrino, allowing the quark to fragment into a charmed hadron, which in turn decays semileptonically producing the second muon. Charmed quarks are assumed to be produced from d-quarks ($\sin^2\theta_c$) and s-quarks ($\cos^2\theta_c$) by neutrinos, and only from $\bar{s}$-quarks ($\cos^2\theta_c$) by antineutrinos. The quark helicities implied by these couplings predict flat y-distributions ($y = \nu/E_\nu$, $\nu = E_\nu - E_{\mu 1}$, where $E_{\mu 1}$ is the energy of the primary muon) for both neutrino- and antineutrino-induced dimuons, apart from threshold effects and experimental cuts. Scaling is assumed to hold (this is approximately true in normal charged-current interactions), but because of the mass correction in the light-to-heavy quark transition, the effective scaling variable becomes

$$\xi = x + \frac{m_c^2}{2 M_N E_\nu y} ,$$

where m_c is the effective mass of the charmed quark (taken to be 1.5 GeV/c^2), M_N is the nucleon mass, and x is the normal scaling variable ($x = Q^2/2 M_N \nu$). After production (unless otherwise noted), the charmed quark is allowed to fragment into a charmed hadron with a uniform fragmentation function, D(z) = constant, where z is the energy of the charmed hadron divided by the energy of the charmed quark. We will also make comparison with other fragmentation

functions. The charmed hadron is given a transverse momentum relative to the direction of the charmed quark according to the distribution $\frac{dN}{dp_\perp^2} \propto e^{-6\sqrt{p_\perp^2+m_c^2}}$. The decay process is approximated by the reaction,

$$c \to s + \ell^+ + \nu_\ell$$

$$\bar{c} \to \bar{s} + \ell^- + \bar{\nu}_\ell,$$

where the Cabibbo suppressed modes have been ignored. The predictions of the Monte Carlo are insensitive to the detailed assumptions.[22] The 4 GeV/c muon momentum cut is also applied to Monte Carlo generated events.

In Figs. 4, 5, and 6, the energy distributions of the primary and secondary muon and the energy asymmetry distribution, $Y = (E_{\mu 1}-E_{\mu 2})/(E_{\mu 1}+E_{\mu 2})$, are shown, along with the sum of the Monte Carlo and background predictions. The agreement is very good. In Fig. 7, the total energy (corrected) distribution and predicted distribution of the events is shown. Note the lack of low energy events, reflecting the combined effects of charm threshold and the 4 GeV/c muon momentum requirement. The kaon neutrino peak is clearly visible. Figure 8 shows the x-distribution. It agrees well with the predicted distribution, being narrower than for CC events. The mean x for CC events is 0.23 ± 0.01, while the mean x for dimuon events is 0.17 ± 0.02. We present the y-distribution in Fig. 9. It shows a depletion of events at low and high y due to the charmed quark threshold combined with our 4 GeV/c muon momentum requirement. For completeness the Q^2, four-momentum transfer squared, and W, hadron invariant mass, distributions are shown in Figs. 10 and 11. The invariant mass distribution of the two muons is presented in Fig. 12. It is broad with no narrow peaks, consistent

with a separate source for the two muons. In Fig. 13, the distribution in ϕ, the angle between the momentum vectors of the two muons projected onto the plane perpendicular to the neutrino direction, is shown. The usual anti-correlation, peaking at 180^{o} in agreement with the predicted distribution, is seen confirming the hadronic source of the second muon. The lack of a peak at 0^{o} demonstrates no large source of heavy leptons.

In Fig. 14, the momentum distribution of the second muon perpendicular to the plane formed by the primary muon and neutrino is shown. It appears to be somewhat broader than the same distribution for hadrons in CC events and the Monte Carlo distribution based on the quark decay model. We present the charged particle multiplicity in Fig. 15.

The distribution in $z_{\mu 2}$, where $z_{\mu 2} = E_{\mu 2}/\nu$, is shown in Fig. 16. This distribution is quite sensitive to the form of the fragmentation function of the charmed quark into a charmed hadron; it doesn't measure the fragmentation function directly since the decay muon carries only a fraction of the charmed hadron energy. The data are in good agreement with the Monte Carlo distribution based on a uniform fragmentation function, which is used to generate our other distributions, but also agree nicely with a $z(1+z)$ distribution. Agreement with a $z^{-1}(1-z)$ distribution is poor as with other distributions which fall this rapidly. See Ref. 22 for a more complete discussion of fragmentation models.

In Fig. 17, the quark fragmentation distributions of all positive tracks, negative tracks, and V^{o}'s from $\mu^{-}\mu^{+}$ dimuon events are shown. The contribution of the second muon to the distribution of positive tracks is shaded. For comparison the same distributions are shown for hadrons from CC events. The distribution of positive tracks from dimuon events falls more slowly than those from normal CC events, as expected from the fragmentation function discussed above.

Finally in Table III, we calculate the means of the distributions presented in the figures and compare them with those predicted by the Monte Carlo. The agreement is good, as is the agreement between the predicted distributions and the observed distributions shown in all figures, consistent with the charm production and decay model for the dimuon events. We point out, however, that the distributions for dimuons and the distributions of the background events are similar.

VII. Summary and Conclusions

We have presented results on a sample of 54 opposite-sign dimuons and 8 like-sign dimuons ($\mu^-\mu^-$) obtained from a 326,000 picture exposure of the Fermilab 15' Bubble Chamber to the Quadrupole Triplet Neutrino Beam. The like-sign dimuons are consistent with background. Subtracting background, we estimate a dimuon to single muon ratio of $(0.39 \pm 0.10) \times 10^{-2}$ for events with muons above 4 GeV/c. Separating the ν-induced and the $\bar{\nu}$-induced dimuons on the basis of the transverse momentum of the muons relative to all non-muon tracks, we find dimuon to single muon ratios of $(0.37 \pm 0.10) \times 10^{-2}$ and $(0.5 \pm 0.3) \times 10^{-2}$ respectively for a muon momentum cut of 4 GeV/c.

The opposite-sign dimuon events contain 10 V^0's. Correcting for background, detection efficiency, and unseen decays, we obtain a neutral strange particle rate per dimuon event of 0.6 ± 0.3.

Lastly we have compared distributions with predicted distributions based on a charm production and decay Monte Carlo. The agreement is good, and no evidence is seen for heavy lepton production.

Acknowledgments

We would like to acknowledge the encouragement and assistance of the staff of FNAL and particularly the 15' Bubble Chamber crew. Our scanning, measuring, and computing people deserve special praise for their careful work on this difficult experiment. We have benefited from conversations with S. Pakvasa and V. Barger. In particular we wish to thank John Wills for an excellent job on our charm Monte Carlo.

This work was supported in part by the Physics Division of the U. S. Department of Energy at Lawrence Berkeley Laboratory (Contract #W-7405-ENG-48), the University of Hawaii, Fermilab, and the University of Wisconsin; and by the National Science Foundation at the Universities of California and Washington. One of us (T.H.B.) acknowledges the support of the A. P. Sloan Foundation.

References

1. A. Benvenuti et al., Phys. Rev. Lett. 34, 419 (1975).
2. A. Benvenuti et al., Phys. Rev. Lett. 35, 1199, 1203, 1249 (1975).
3. B. C. Barish et al., Phys. Rev. Lett. 36, 939 (1976); 39, 981 (1977).
4. M. Holder et al., Phys. Lett. 69B, 377 (1977).
5. A. Benvenuti et al., Phys. Rev. Lett. 41, 725 (1978).
6. A. Benvenuti et al., Phys. Rev. Lett. 41, 1204 (1978).
7. C. T. Murphy, Proceedings of the XIIth Recontre De Moriond, Les Arcs, Savoie, France, p. 301 (1977).
8. P. Bosetti et al., Phys. Lett. 73B, 380 (1978).
9. F. A. Harris, Proceedings of the Oxford Conference on Neutrino Physics at Accelerators, Oxford, England, p. 209 (1978); V. Z. Peterson, Proceedings of the XIX International Conference on High Energy Physics, Tokyo, Japan, p. 352 (1978).
10. J. von Krogh et al., Phys. Rev. Lett. 36, 710 (1976) and P. Bosetti et al., Phys. Rev. Lett. 38, 1248 (1977).
11. J. Blietschau et al., Phys. Lett. 60B, 207 (1976).
12. C. Baltay et al., Phys. Rev. Lett. 39, 62 (1977).
13. H. C. Ballagh et al., Phys. Rev. Lett. 39, 1650 (1977).
14. P. Berge et al., Phys. Lett. 81B, 89 (1979).
15. M. L. Stevenson, Proceedings of the Oxford Conference on Neutrino Physics at Accelerators, Oxford, England, p. 362 (1978).
16. R. J. Cence et al., Nucl. Instr. and Meth. 138, 245 (1976).
17. R. Stefanski, private communication.

18. Both TVGP and HYDRA geometry programs are used with very similar results.

19. The kaon fraction is estimated assuming that the number of charged kaons is equal to the corrected number of neutral kaons in the charged-current events. The proton fraction is obtained from: T. H. Burnett et al., Phys. Lett. 77B, 443 (1978); W. M. Yeager et al., Phys. Rev. D16, 1294 (1977).

20. An independent calculation, which uses a Monte Carlo program to generate hadron showers in the EMI absorber, has been used to estimate punch thru background and agrees very well with the method described here. We thank AI Grant for supplying us with his program.

21. Fermilab-IHEP-ITEP-Michigan Neutrino Group, Phys. Rev. Lett. 39, 382 (1977).

22. C.-H. Lai, Phys. Rev. D18, 1422 (1978).

Table Captions

Table I Dimuon candidates and backgrounds (muon momenta > 4 GeV/c).

Table II Summary of V^0 characteristics for opposite-sign dimuons. Events with weight of zero occur within 1 cm of primary vertex.

Table III Comparison of mean values for neutrino induced dimuons ($\mu^-\mu^+$), Monte Carlo dimuon events, and neutrino charged-current events. The dimuon mean is calculated from the sample mean and the background mean. Numbers marked with * are calculated using hadrons with P > 4 GeV/c.

Table I

	$\mu^+\mu^+$	$\mu^+\mu^-$ & $\mu^-\mu^+$	$\mu^-\mu^-$
Events	0	54	8
π and K Decays	0.9 ± 0.2	11.7 ± 2.3	4.0 ± 0.8
Punch Thru	0.2 ± 0.1	6.2 ± 3.1	2.7 ± 1.3
Net Signal	-1.1 ± 1.0	36.1 ± 8.3	1.3 ± 3.2

Table II

Event	Type	V^0 Type	χ^2 for K Hypothesis	χ^2 for Λ Hypothesis	Weight	P fitted (GeV/c)	# Lifetimes	$M_{\mu 2V}$
14730594	$\mu^-\mu^+$	K^0	3.2	---	1.6	12.8	.05	1.15
14791740	$\mu^-\mu^+$	K^0	4.8	---	3.0	39.3	.04	1.43
15101414	$\mu^-\mu^+$	Λ^0	---	1.5	1.6	.54	.79	7.03
15560114	$\mu^-\mu^+$	K^0	1.1	---	3.5	54.5	.11	1.67
15690673	$\mu^+\mu^-$	K^0	0.8	---	1.6	6.1	.78	1.97
15761797	$\mu^-\mu^+$	K^0	0.67	---	2.7	12.9	.27	0.99
16051203	$\mu^-\mu^+$	K^0	0.2	---	0.	2.2	.03	1.34
16420642	$\mu^-\mu^+$	K^0	0.8	---	0.	2.8	.07	1.04
16460680	$\mu^-\mu^+$	K^0	1.7	---	1.6	3.1	.12	1.11
16511246	$\mu^-\mu^+$	Λ^0	---	11.6	1.6	3.7	1.3	2.63

Table III

Variable	Sample Mean	Background Mean	Dimuon Mean	Monte Carlo Mean	Neutrino CC Mean
$E_{\mu 1}$ (GeV)	47.9 ± 6.8	48.3 ± 3.0	47.7 ± 8.8	45.2 ± 1.2	49.9 ± 1.7
$E_{\mu 2}$ (GeV)	12.9 ± 1.3	10.8 ± 0.6	14.4 ± 1.6	13.1 ± 0.31	---
$Y = (E_{\mu 1}-E_{\mu 2})/(E_{\mu 1}+E_{\mu 2})$	0.39 ± 0.06	0.47 ± 0.03	0.33 ± 0.07	0.40 ± 0.01	---
E_ν (GeV)	121. ± 10.	107. ± 4.1	130. ± 13.4	118. ± 1.8	86.4 ± 2.2
x	0.18 ± 0.02	0.20 ± 0.01	0.17 ± 0.02	0.18 ± .00	0.23 ± 0.01
y	0.60 ± 0.04	0.57 ± 0.02	0.62 ± 0.05	0.63 ± 0.07	0.45 ± 0.01
Q^2 (GeV^2/c^2)	23.2 ± 3.6	17.6 ± 1.2	27.0 ± 5.3	20.0 ± 0.6	14.6 ± 0.7
W (GeV/c^2)	9.65 ± 0.57	8.55 ± 0.23	10.4 ± 0.76	10.1 ± 0.1	6.54 ± 0.12
$M_{\mu\mu}$ (GeV/c^2)	3.06 ± 0.31	2.93 ± 0.11	3.14 ± 0.45	2.98 ± 0.03	---
ϕ (degrees)	134. ± 6.5°	144. ± 2.6°	127. ± 8.6°	141. ± 0.7	140. ± 1.4*
$p_{\mu 2}^{L\mu\nu}$	0.33 ± 0.04	0.26 ± 0.02	0.38 ± 0.05	0.28 ± 0.01	0.29 ± 0.01*
Charged multiplicity	8.50 ± 0.49	7.53 ± 0.19	9.16 ± 0.64	---	6.67 ± 0.11
$z_{\mu 2}$ - constant	0.24 ± 0.02	0.25 ± 0.01	0.24 ± 0.03	0.20 ± 0.00	---
$z_{\mu 2}$ - $z(z+1)$	0.24 ± 0.02	0.25 ± 0.01	0.24 ± 0.03	0.35 ± 0.00	---

Figure Captions

Fig. 1 Plan and elevation views of the Fermilab 15' Bubble Chamber, Internal Picket Fence (IPF), and Two-Plane External Muon Identifier. The partial IPF was tested during this experiment but was not used in this analysis.

Fig. 2 Neutrino spectrum (arbitrary scale). The curves are for 400 GeV/c protons incident on the target with the Quadrupole Triplet set to focus 200 GeV/c positive secondaries.

Fig. 3 Plot showing the transverse momentum relative to all non-muon tracks of the primary muon versus that of the secondary muon. For this plot the primary muon, meaning the one coming from the neutrino vertex, is chosen as the muon with the largest value of this transverse momentum. Circles are for events where the primary muon is negative; crosses (+) are for events where the primary muon is positive. For events near the diagonal (between dashed lines), the selection is ambiguous. For these ambiguous events on all other plots, we select the negative muon as the primary one.

Fig. 4 Number of events (weighted) versus the energy of the primary muon. Shaded events are those selected as antineutrino induced. The full histogram is the total of neutrino and antineutrino induced events. The lower smooth curve (...) is the predicted distribution of events obtained from the Monte Carlo and normalized to the estimated number of dimuons in the sample. The upper curve (---) is the sum of the Monte Carlo distribution and the predicted distribution of background events normalized to the total number of events.

Fig. 5 Number of events (weighted) versus the energy of the secondary muon.

Fig. 6 Number of events (weighted) versus energy asymmetry, $\gamma = (E_{\mu 1}-E_{\mu 2})/(E_{\mu 1}+E_{\mu 2})$.

Fig. 7 Number of events (weighted) versus corrected neutrino energy.

Fig. 8 Number of events (weighted) versus x. $x = Q^2/2M_N\nu$, where Q^2 is the four-momentum transfer squared, M_N is the nucleon mass, and $\nu = E_\nu - E_{\mu 1}$.

Fig. 9 Number of events (weighted) versus y, where $y = \nu/E_\nu$.

Fig. 10 Number of events (weighted) versus Q^2, the four-momentum transfer squared.

Fig. 11 Number of events (weighted) versus W, the invariant mass of the hadron system.

Fig. 12 Number of events (weighted) versus the dimuon invariant mass.

Fig. 13 Number of events (weighted) versus ϕ, the angle between the two muons in a plane perpendicular to the neutrino direction.

Fig. 14 The number of events (weighted) versus the momentum of the second muon perpendicular to the plane formed by the neutrino and the primary muon. The (broken) lines have the same interpretation as in previous plots. The solid curve is the distribution of momentum perpendicular to the μ-ν plane for hadrons above 4 GeV/c from our charged-current events.

Fig. 15 The number of events (weighted) versus the number of charged tracks. The smooth curve is the charged multiplicity distribution of the charged-current events.

Fig. 16 Number of events (weighted) versus $z_{\mu 2}$, where $z_{\mu 2} = E_{\mu 2}/\nu$. Also shown are the Monte Carlo predictions for a uniform fragmentation

function (signified by dashed curve), which is used to generate our other distributions, a z (1+z) distribution (solid curve), and a z^{-1} (1-z) distribution (dash-dot curve).

Fig. 17 The distribution in z (z = E/ν) of (a) V^0's, (b) negatively-charged tracks, and (c) positively-charged tracks in neutrino-induced dimuon events. The contributions of Λ^0's in (a) and of the secondary muon in (c) are shown shaded. The smooth curves are the corresponding z distributions from ν charged-current events.

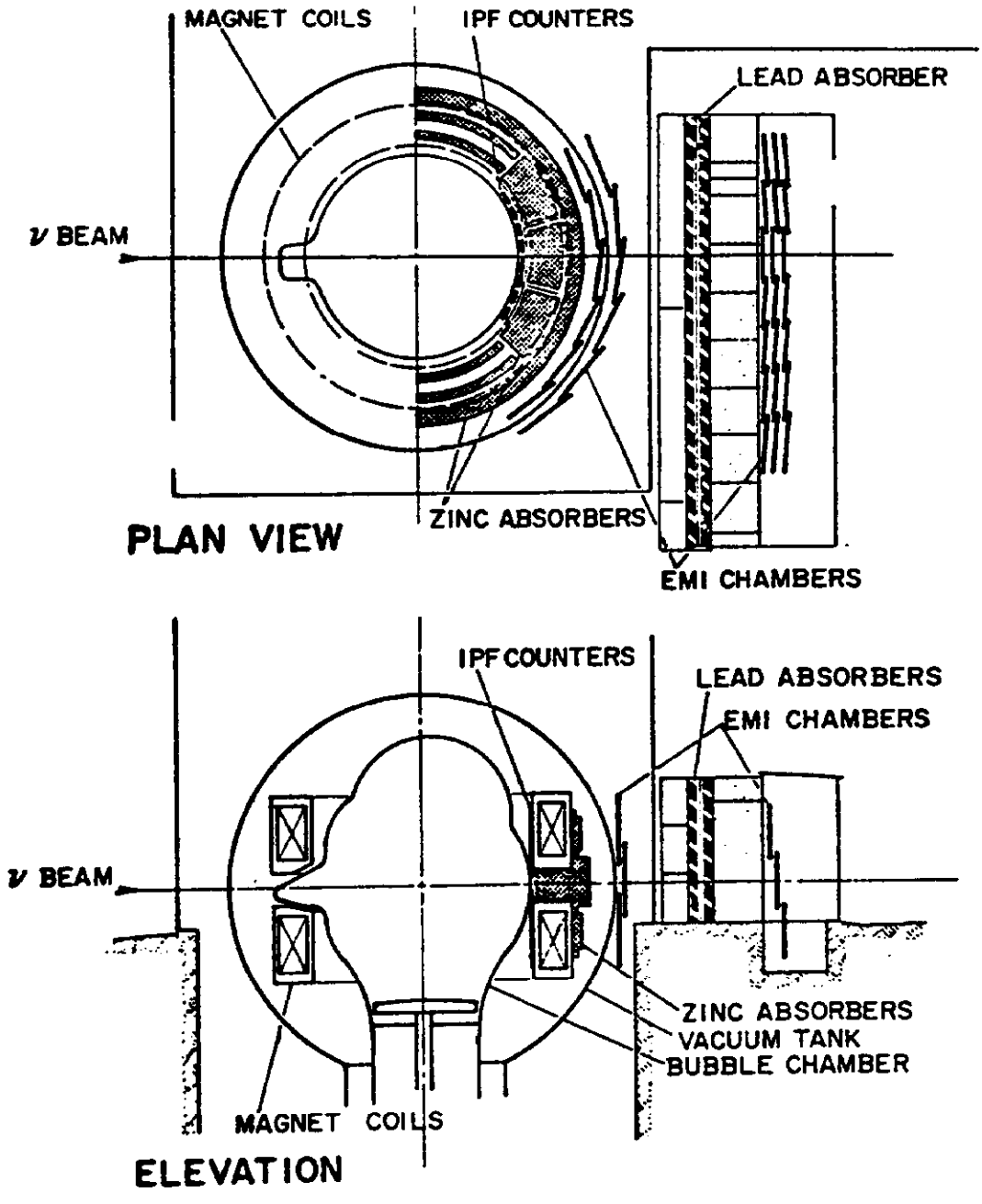
MAGNET COILS
IPF COUNTERS
LEAD ABSORBER
ν BEAM
ZINC ABSORBERS
PLAN VIEW
EMI CHAMBERS
IPF COUNTERS
LEAD ABSORBERS
EMI CHAMBERS
ν BEAM
ZINC ABSORBERS
VACUUM TANK
BUBBLE CHAMBER
MAGNET COILS
ELEVATION

Fig. 1

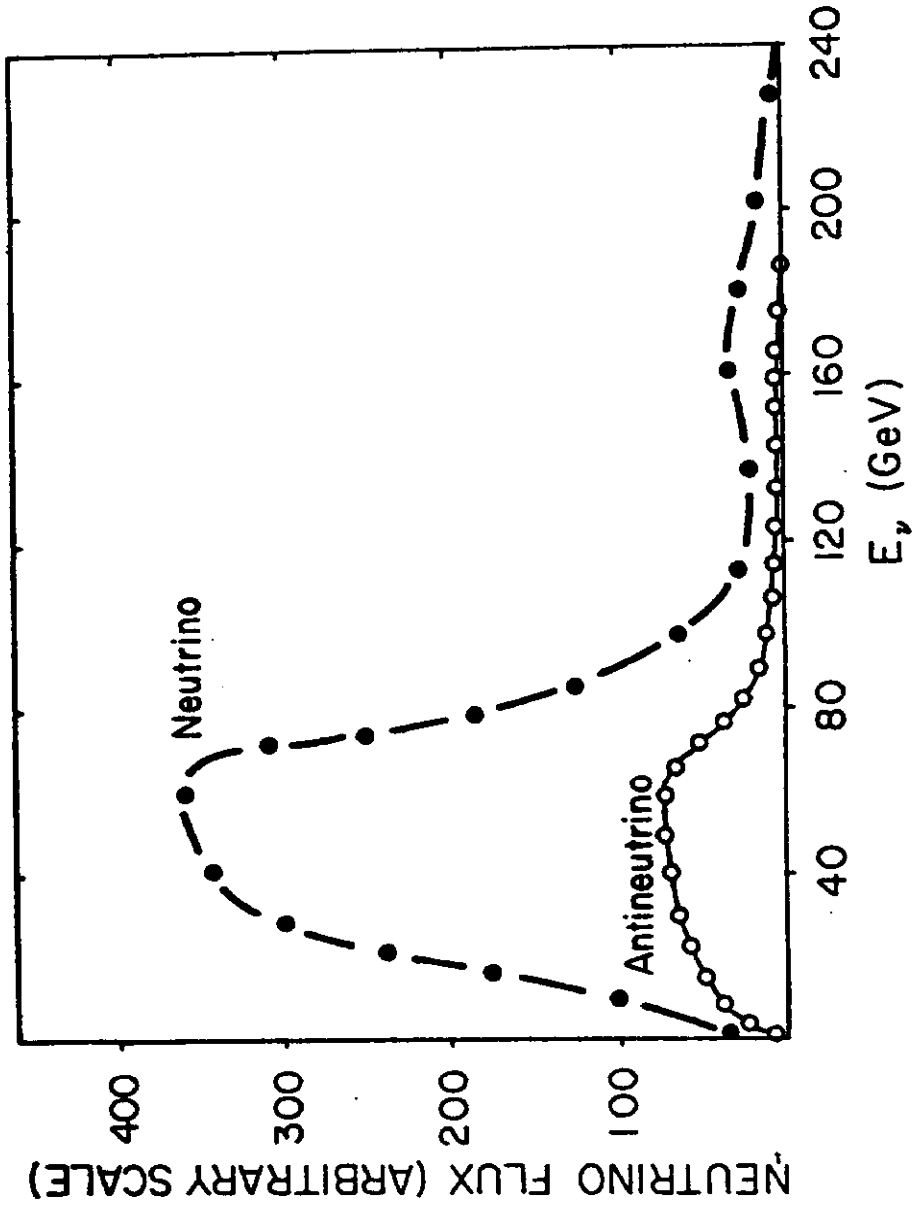
NEUTRINO FLUX (ARBITRARY SCALE)
400
300
200
100
Neutrino
Antineutrino
40
80
120
160
200
240
E$_\nu$ (GeV)

Fig. 2

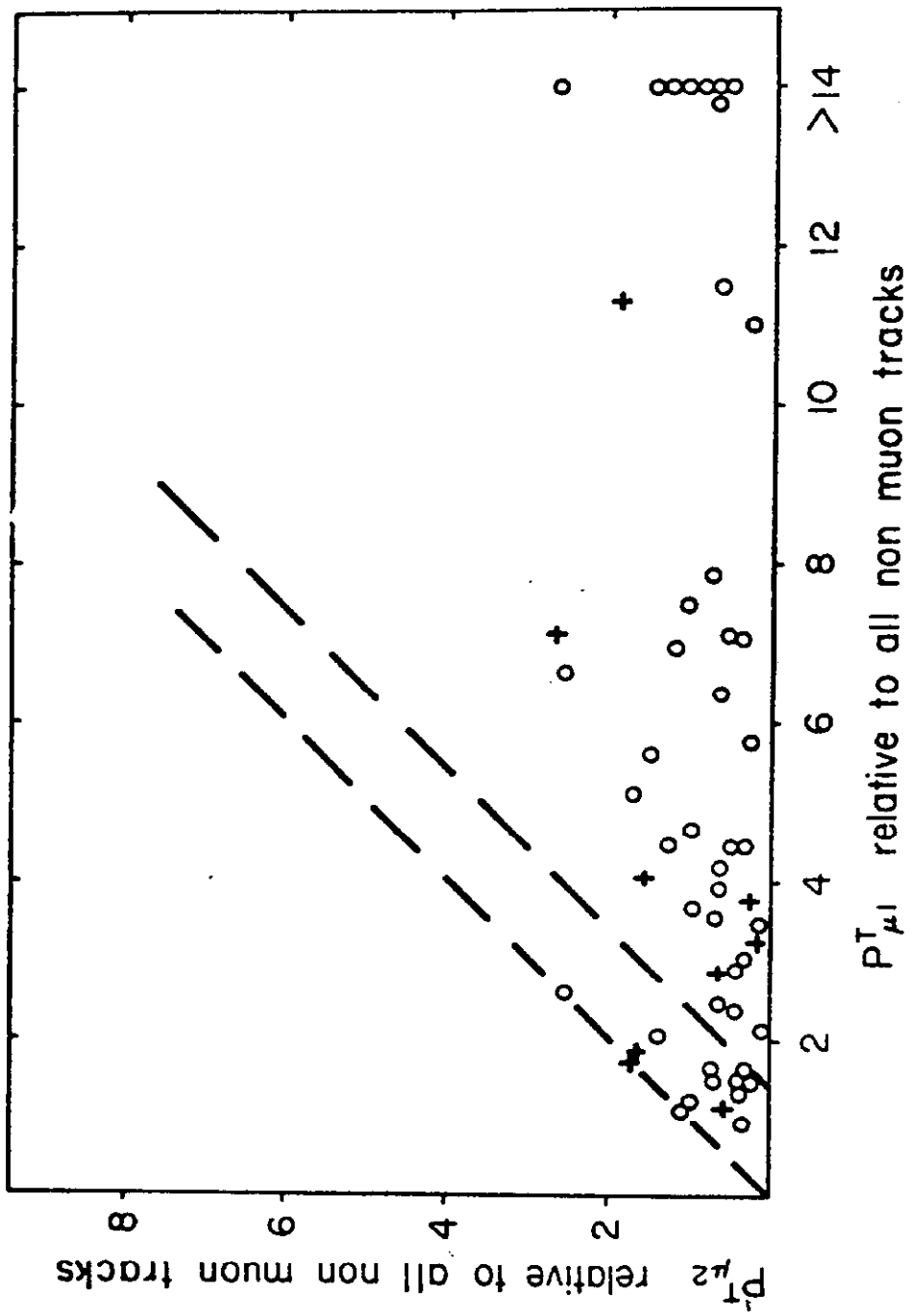
$P_{T_{\mu 2}}$ relative to all non muon tracks
$P^T_{\mu 1}$ relative to all non muon tracks
2
4
6
8
10
12
>14

Fig. 3

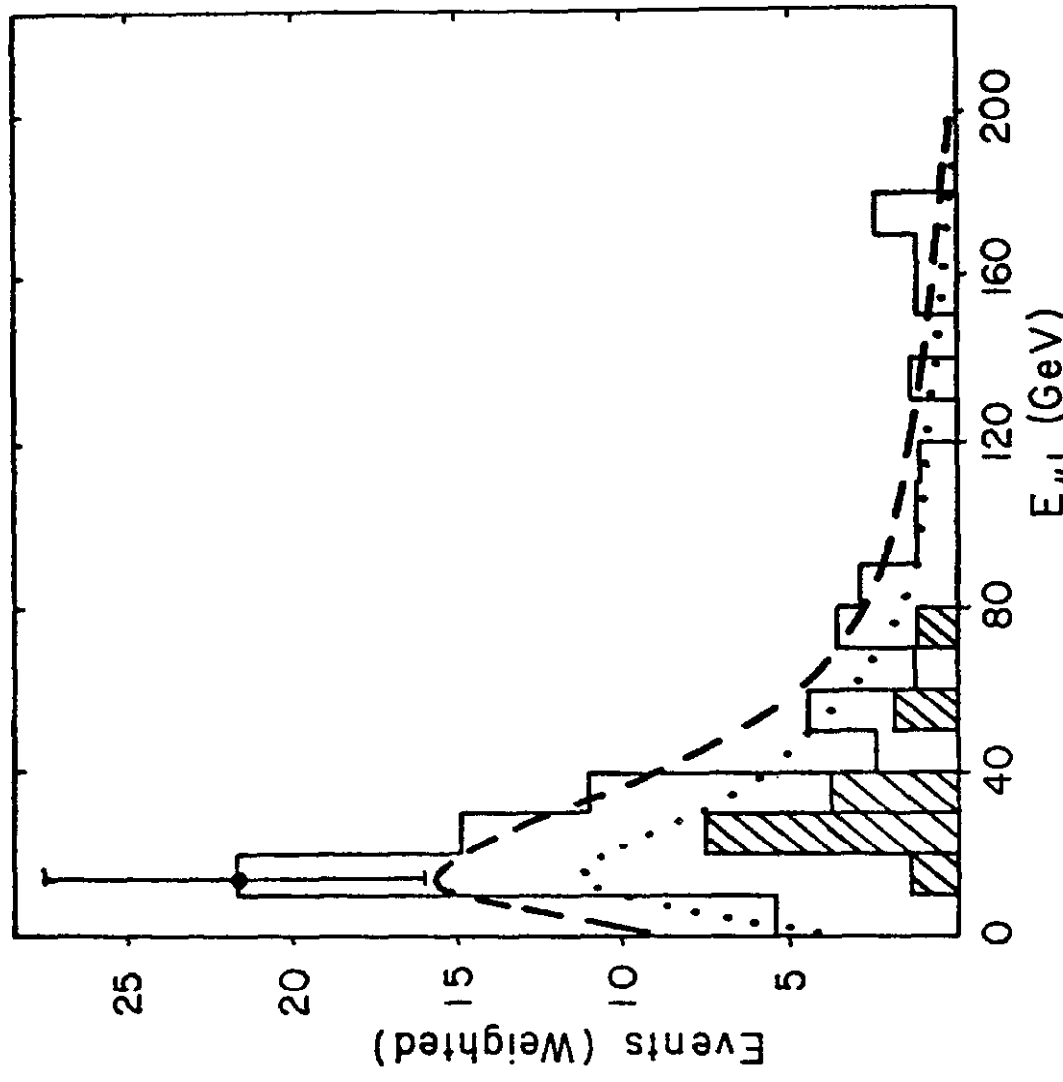

Fig. 4

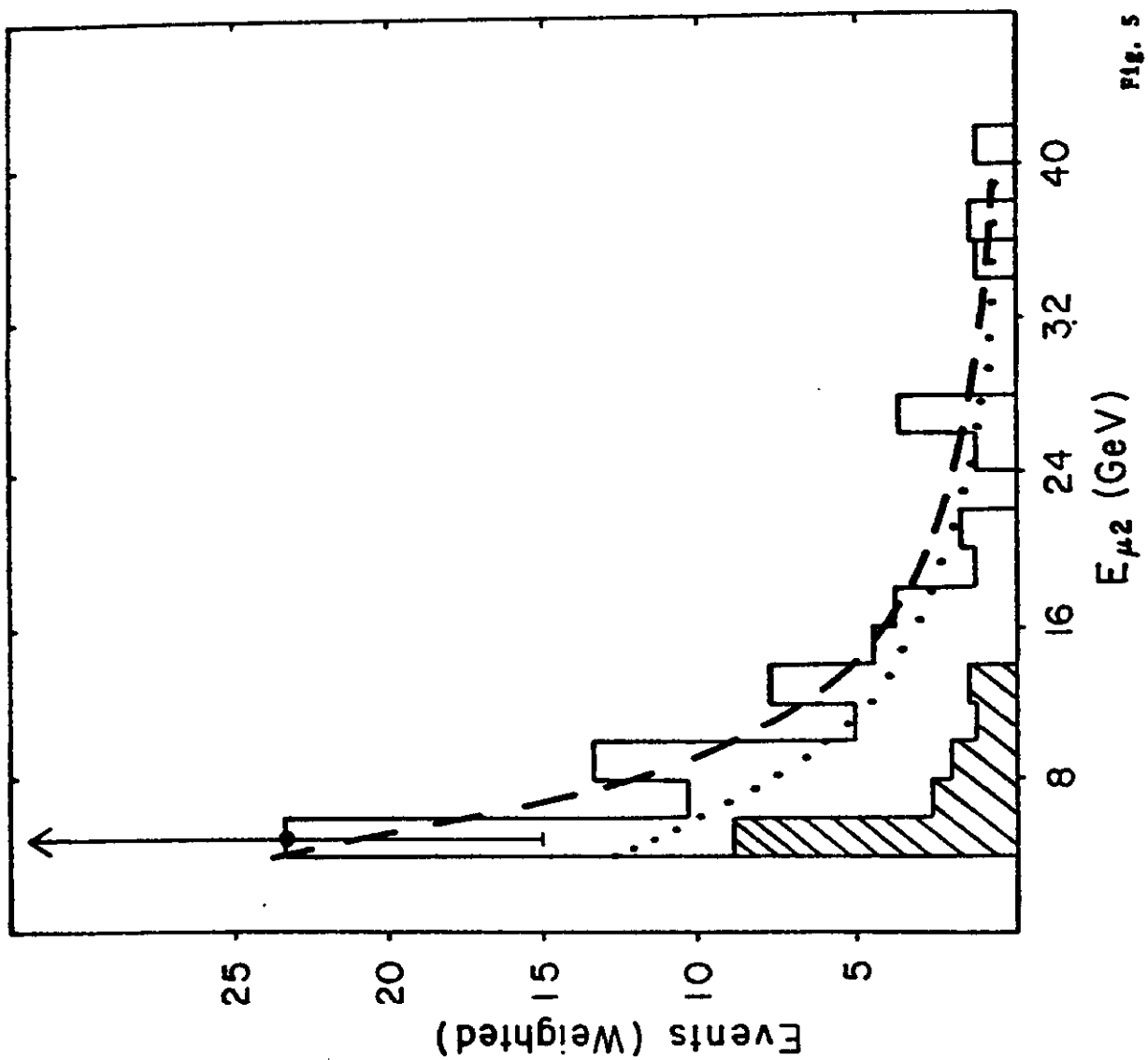

Fig. 5

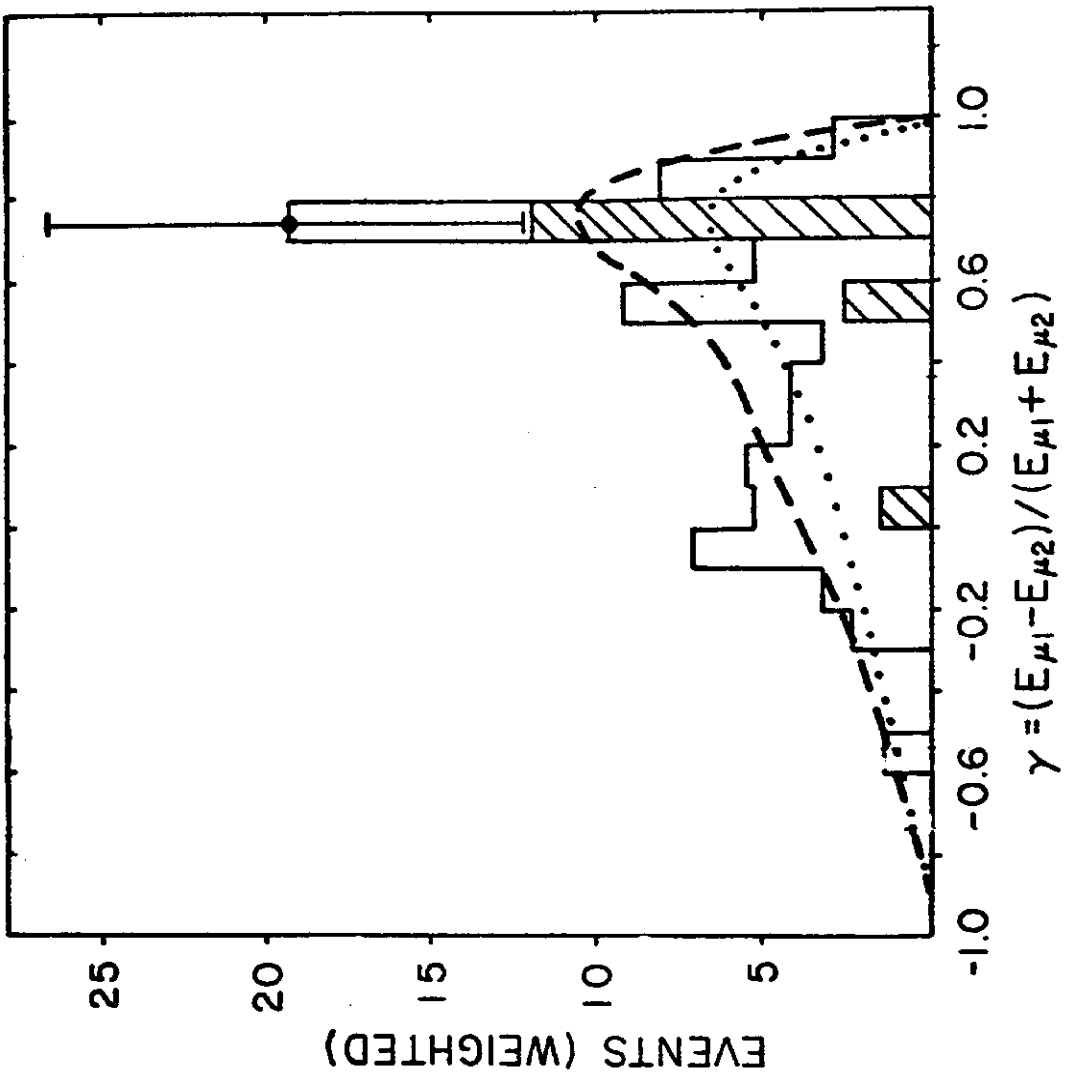
EVENTS (WEIGHTED)
25
20
15
10
5
-1.0
-0.6
-0.2
0.2
0.6
1.0
$\gamma = (E_{\mu 1} - E_{\mu 2})/(E_{\mu 1} + E_{\mu 2})$

Fig. 6

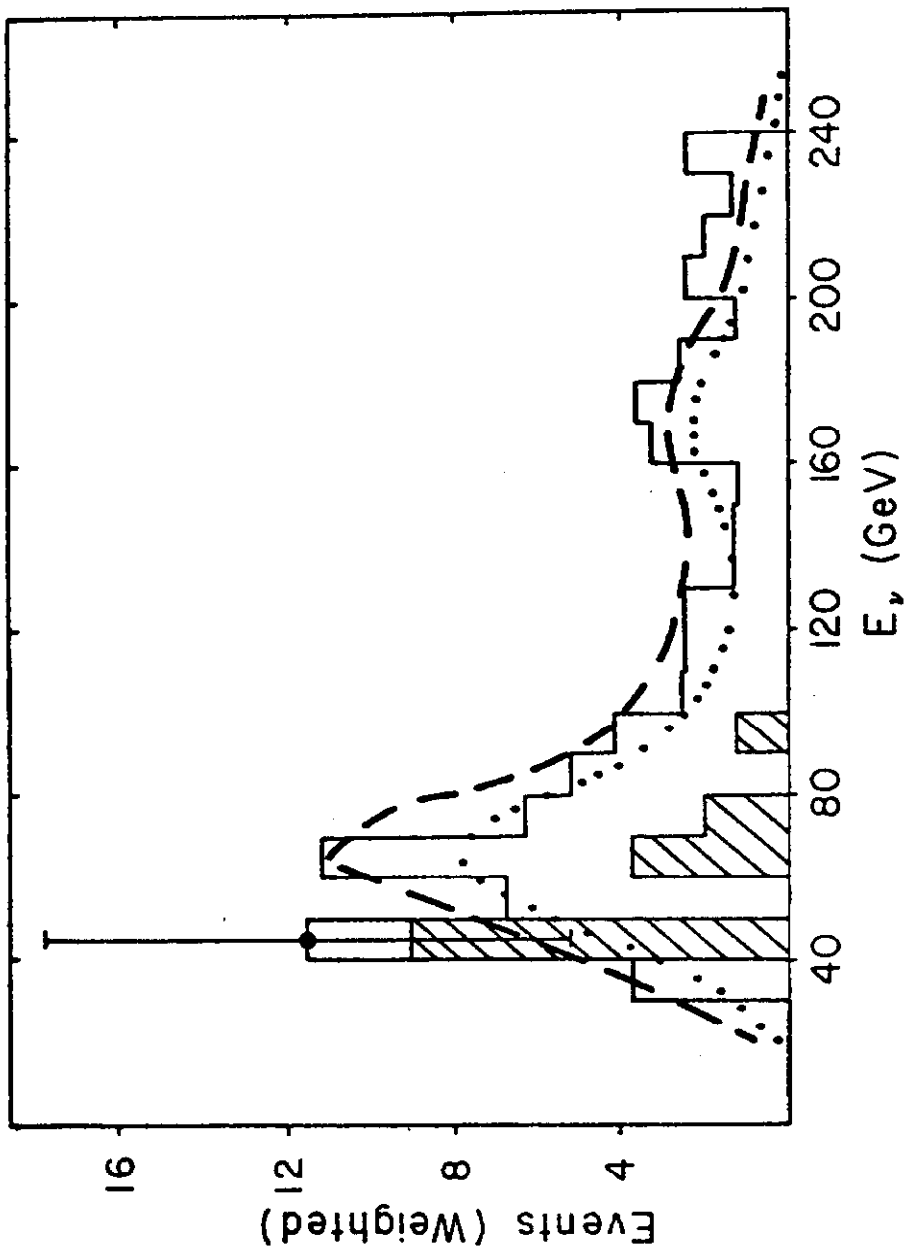

Fig. 7

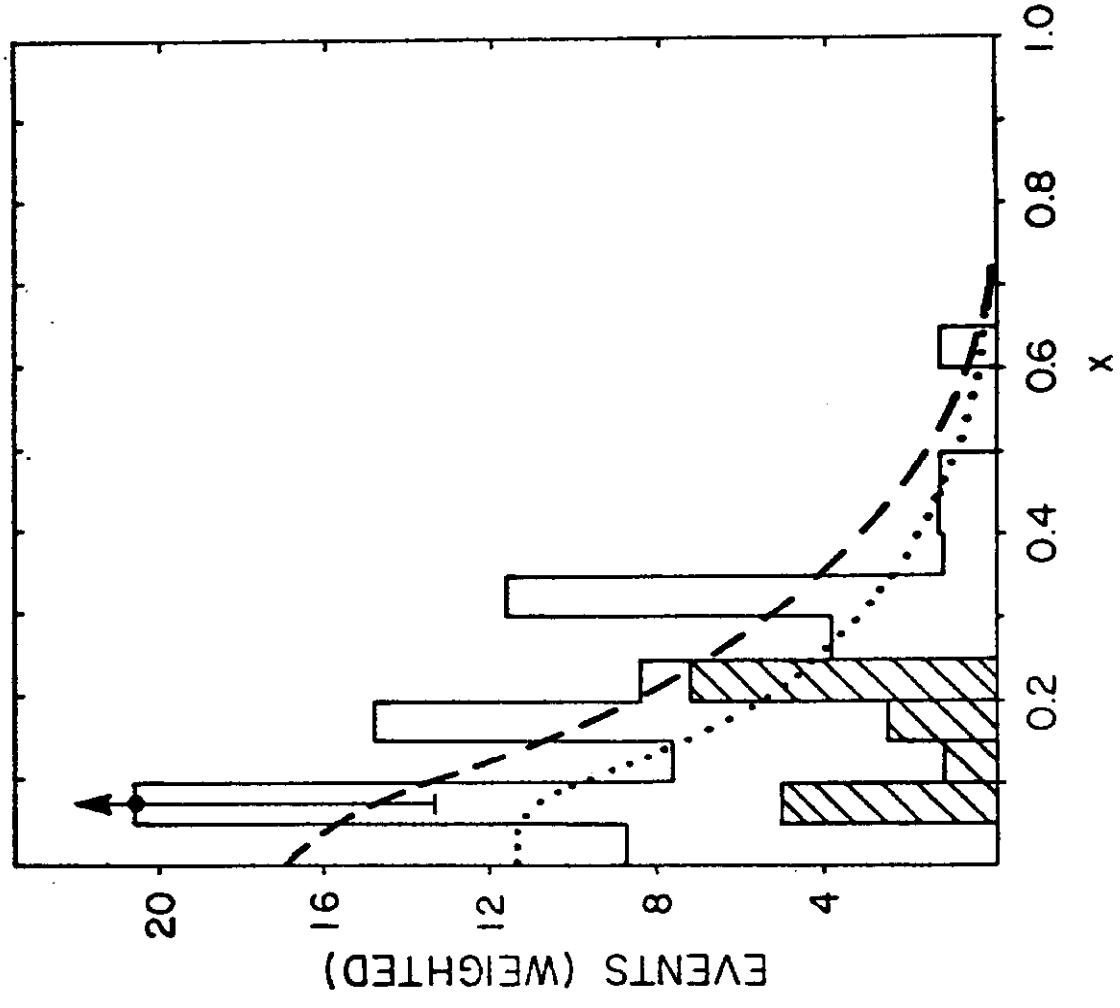

Fig. 8

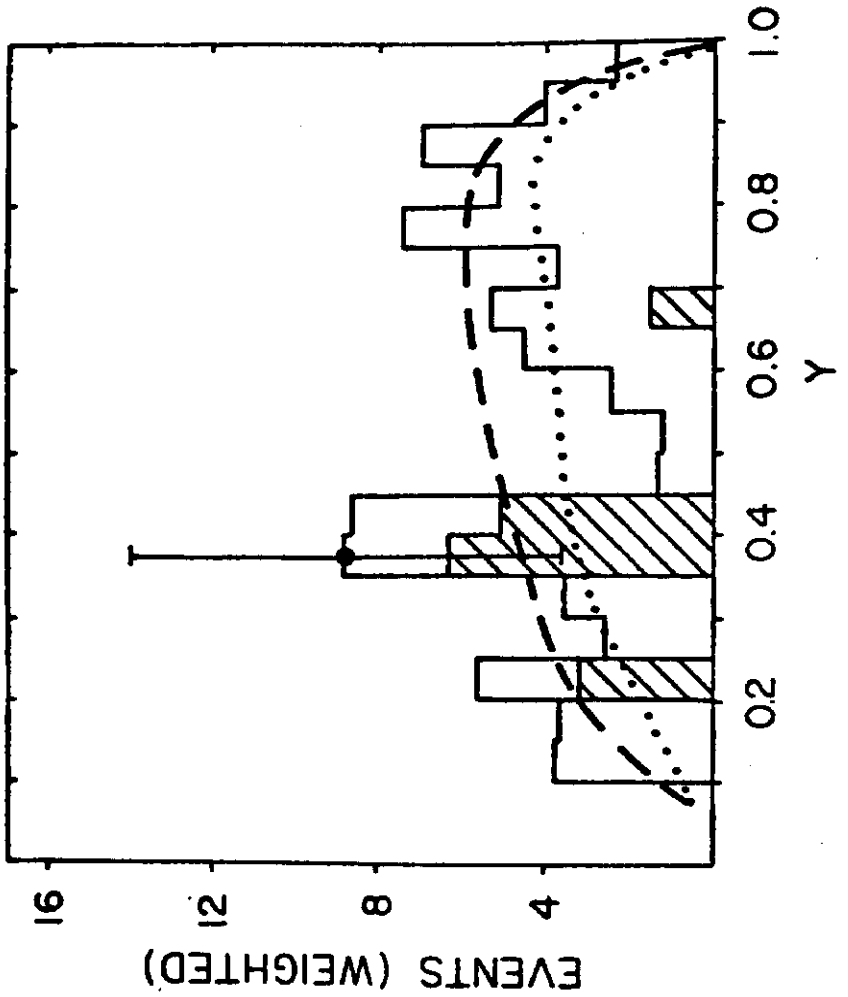

Fig. 9

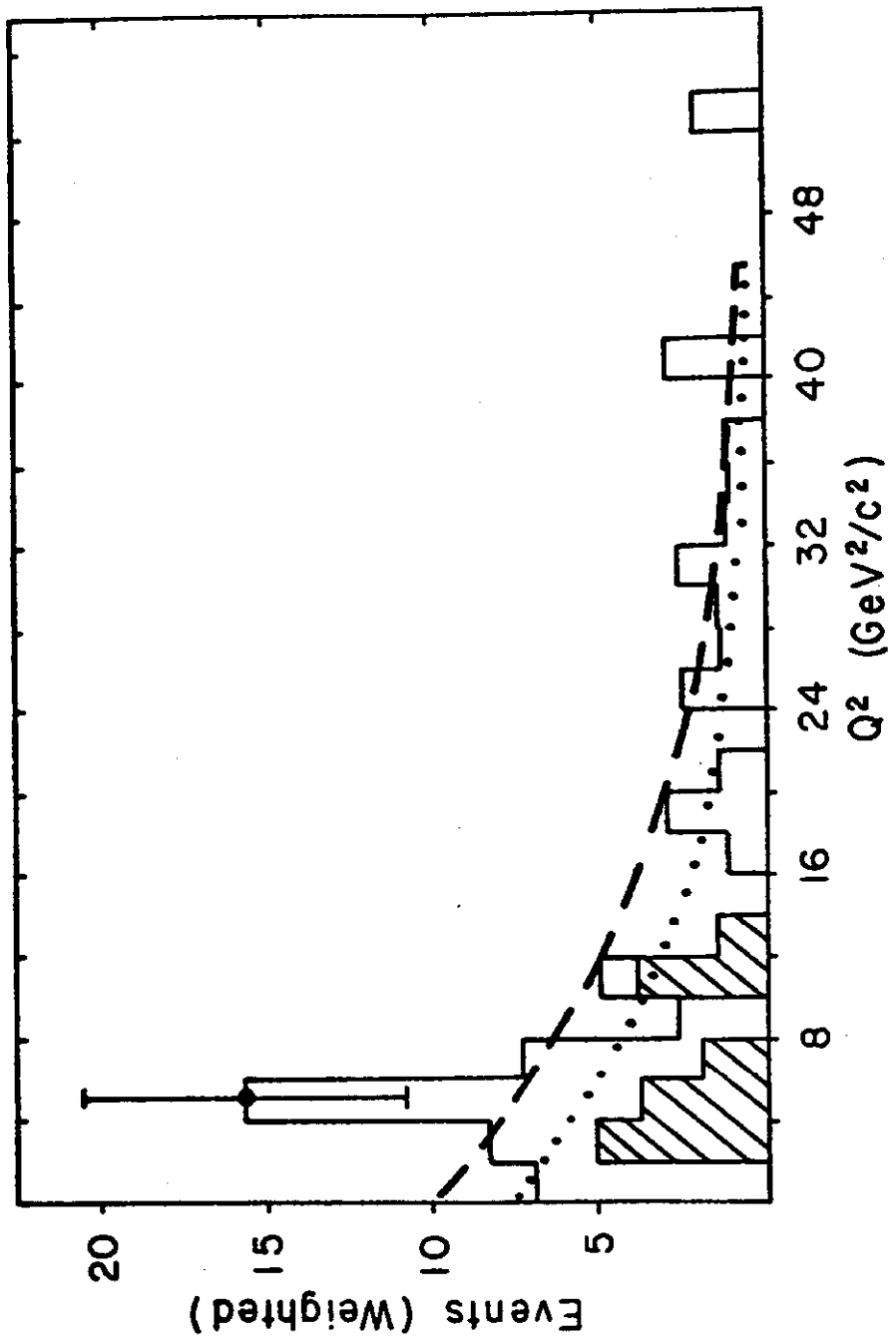

Fig. 10

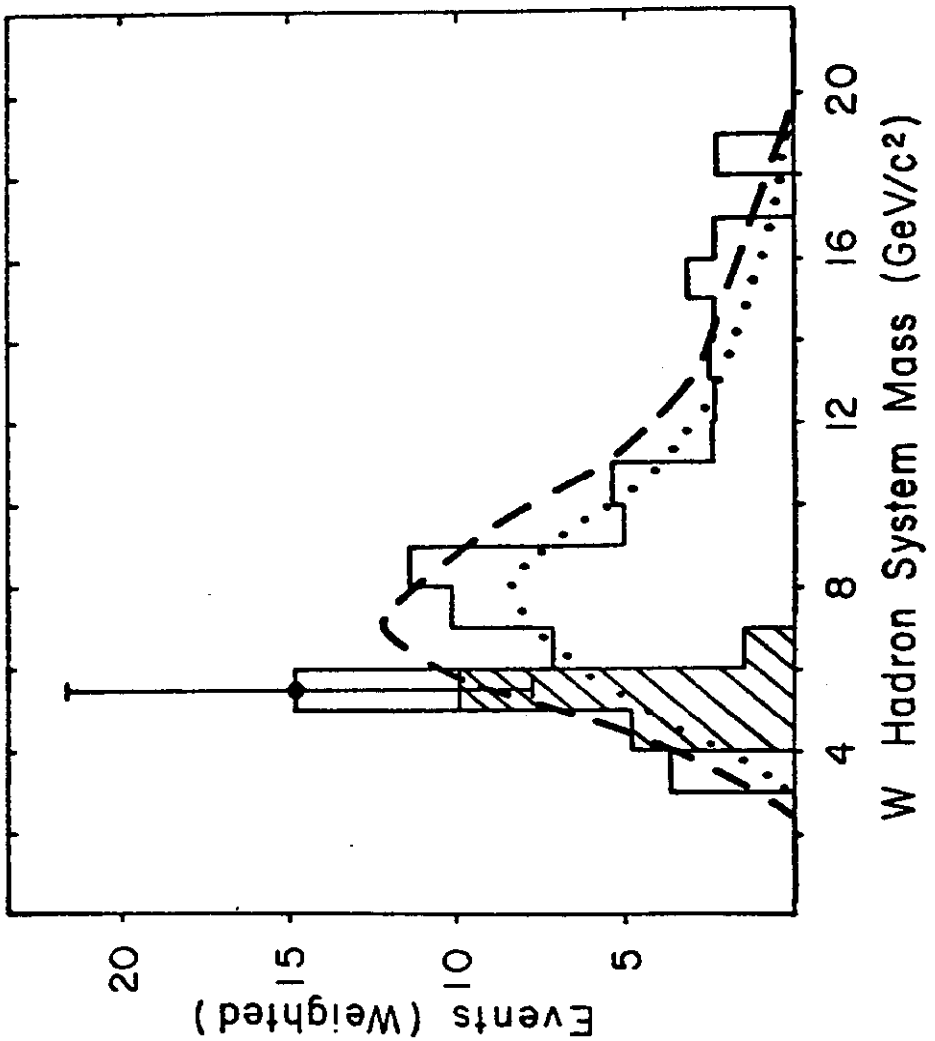
Events (Weighted)
20
15
10
5
4
8
12
16
20
W Hadron System Mass (GeV/c²)

Fig. 11

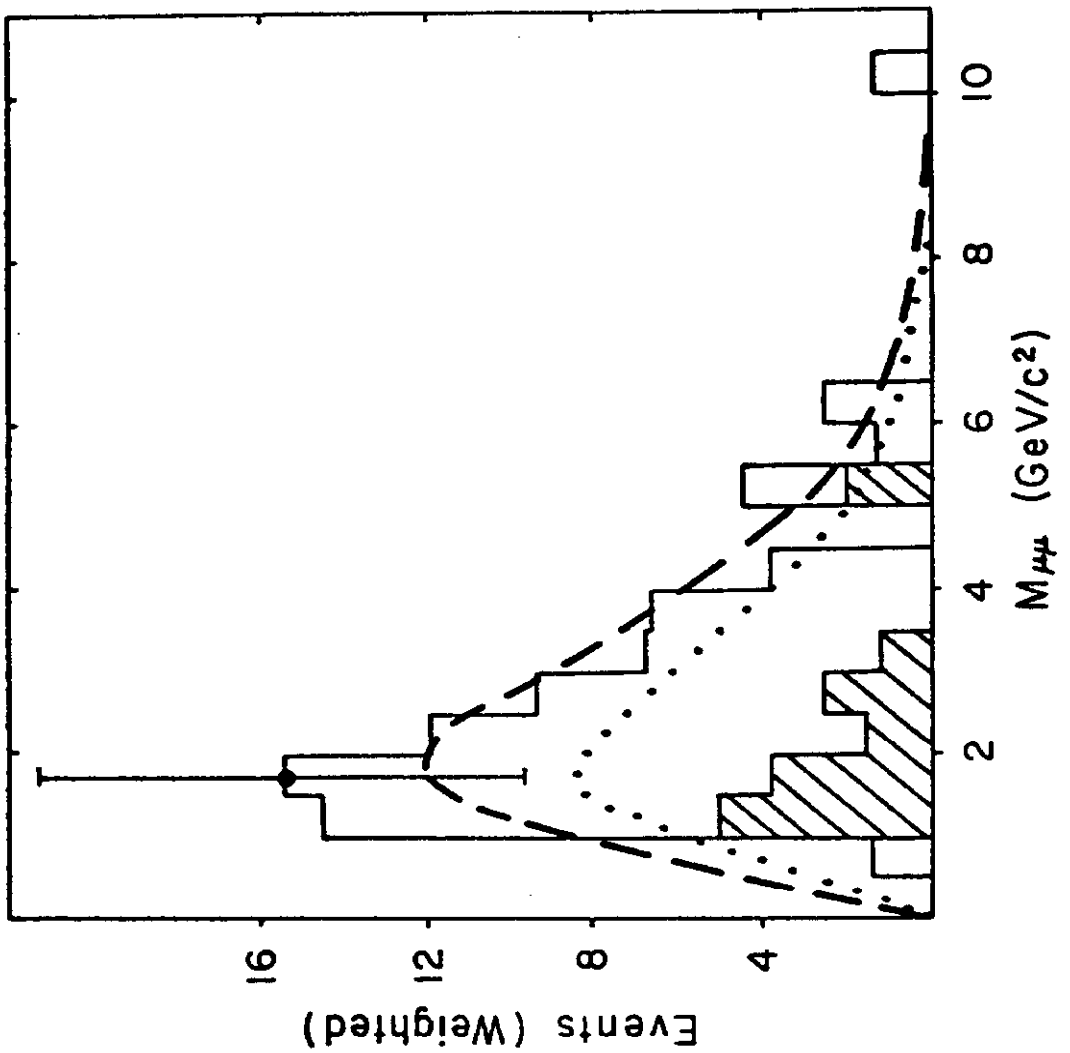

Fig. 12

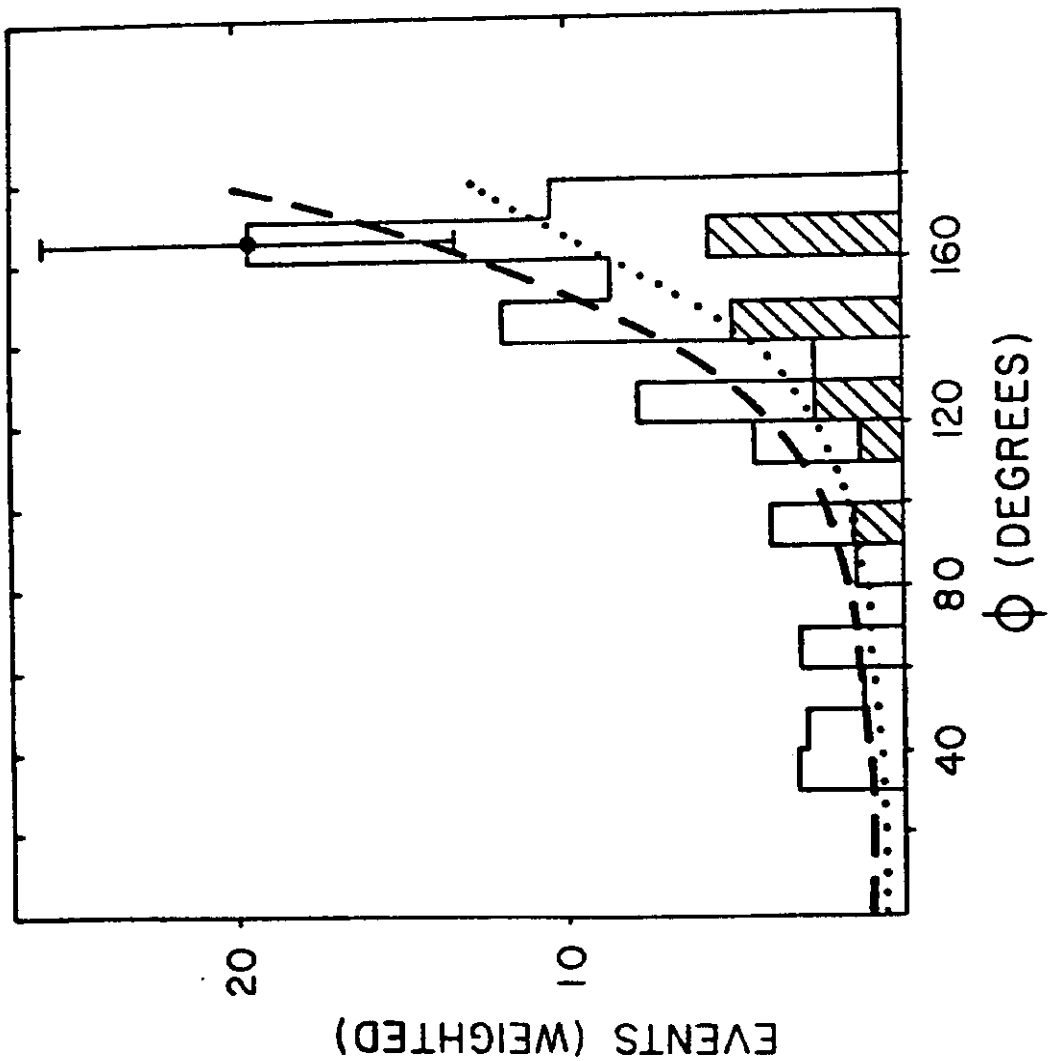

Fig. 13

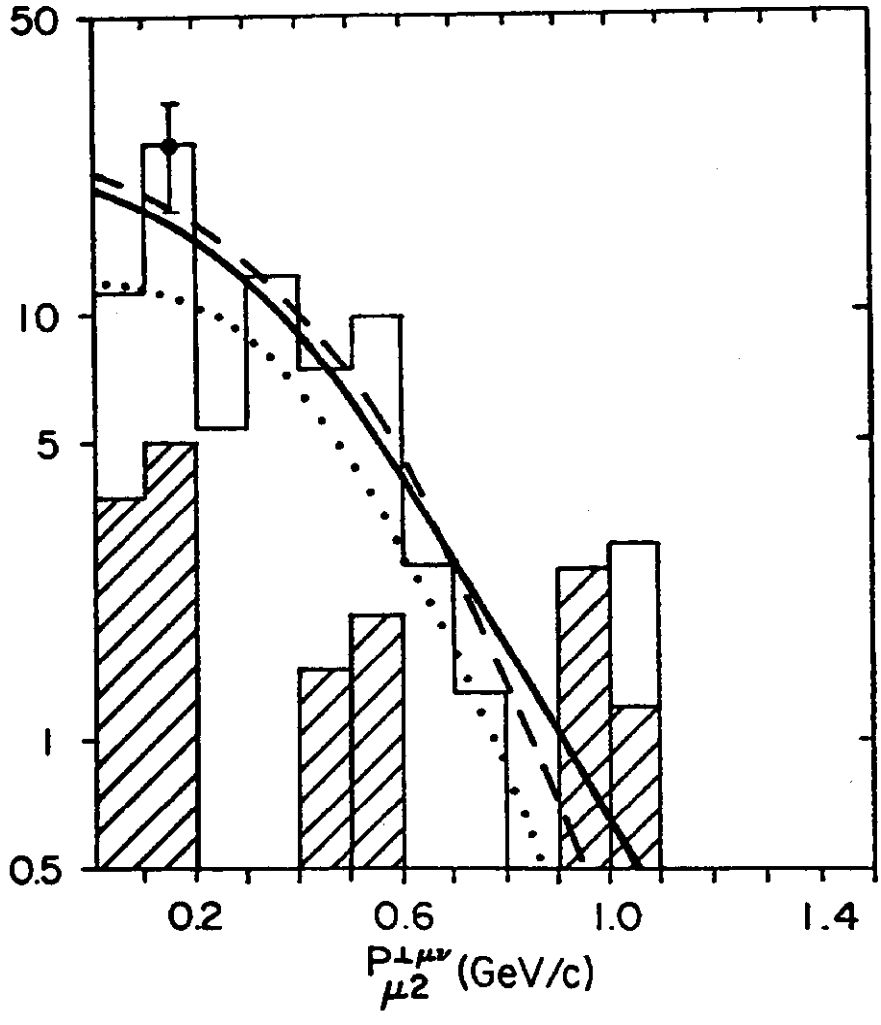

Fig. 14

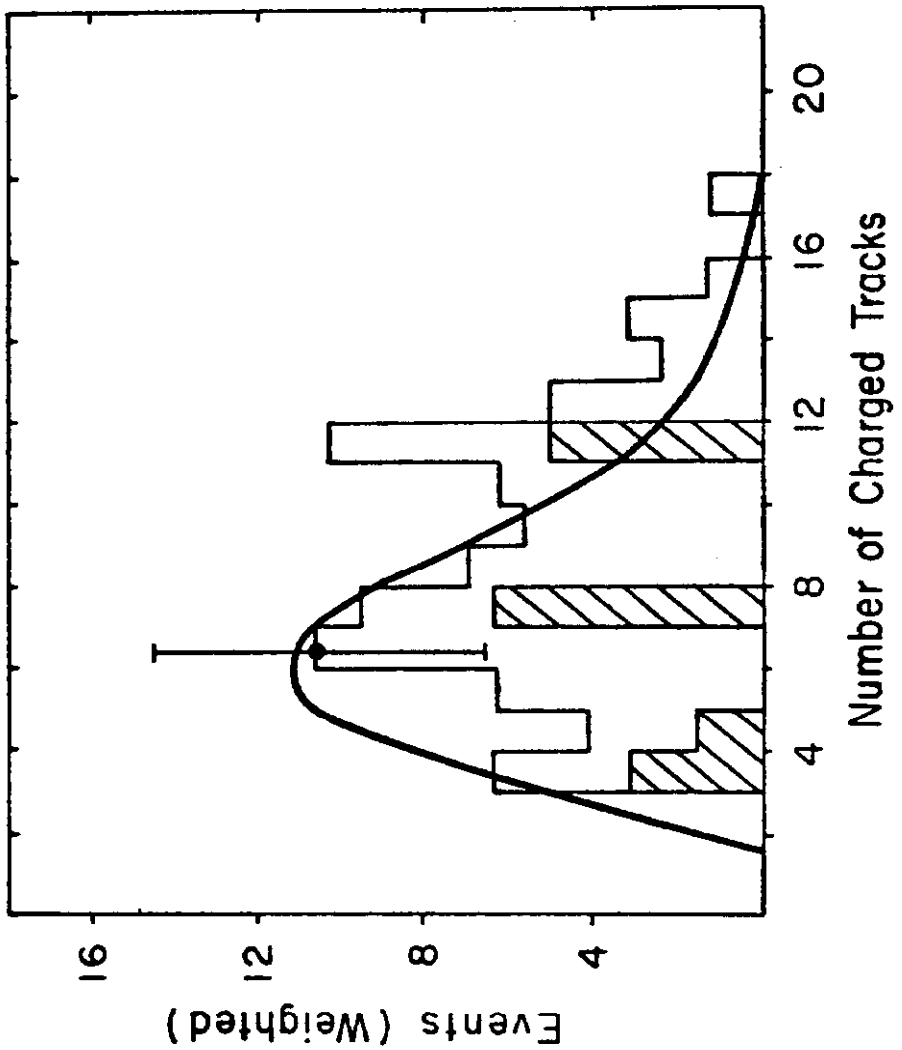

Fig. 15

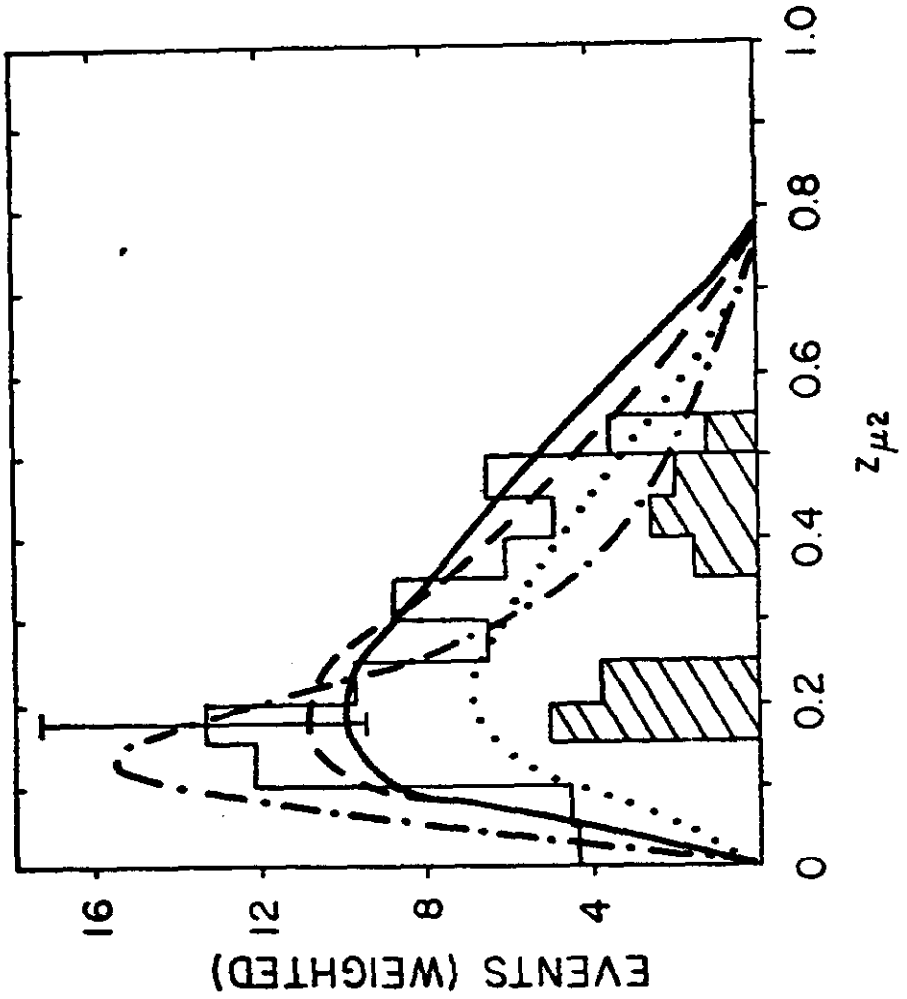

Fig. 16

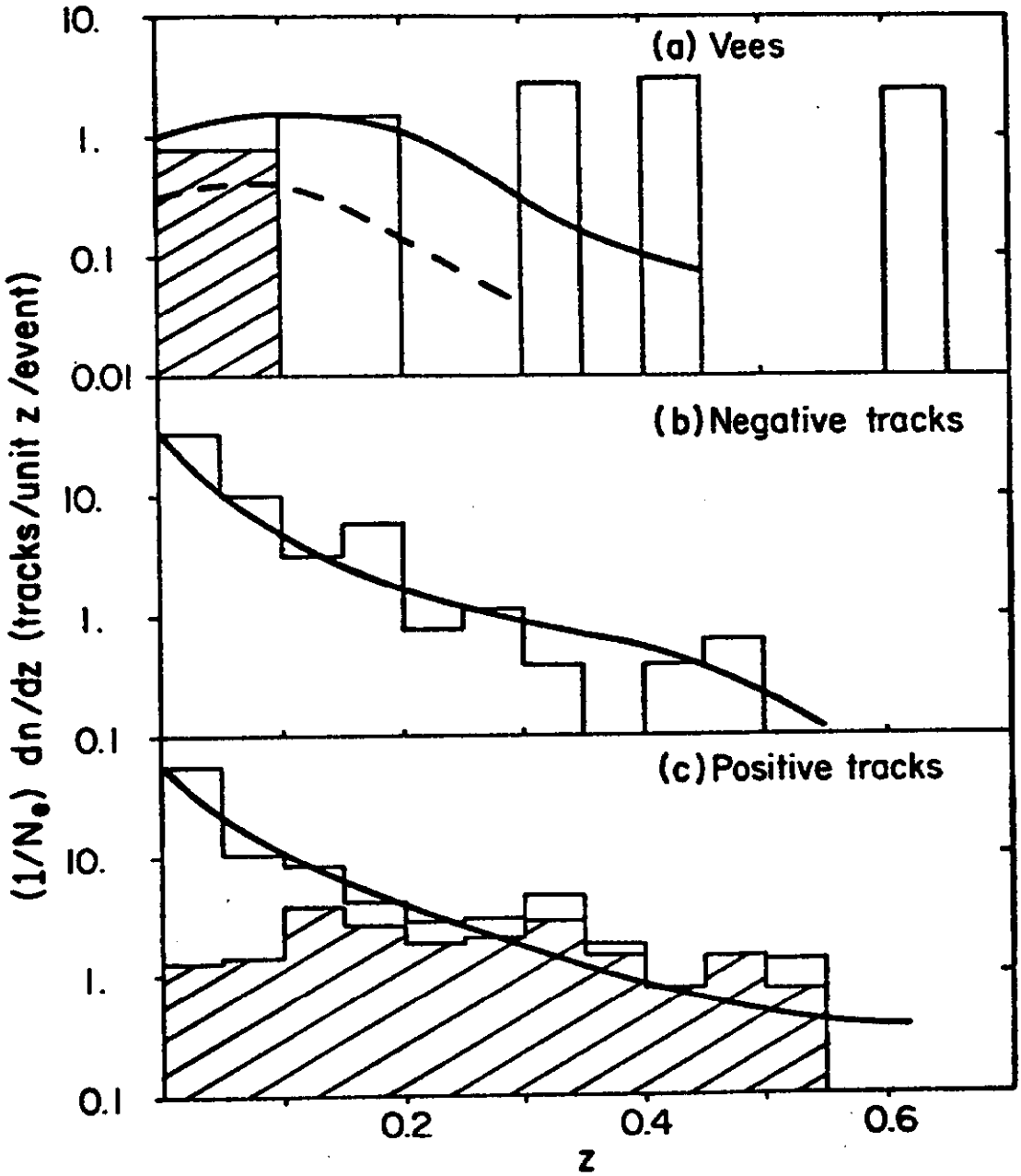
(a) Vees
(b) Negative tracks
(c) Positive tracks
10.
1.
0.1
0.01
10.
1.
0.1
10.
1.
0.1
0.2
0.4
0.6
z
(1/N) dn/dz (tracks/unit z /event)

Fig. 17